Magnetic Resonance Driven Electrical Impedance Tomography: A Phantom Study

M. Negishi[1] and R. T. Constable[2]
[1]*Department of Diagnostic Radiology, Yale University, Connecticut, U.S.A.*
[2]*Departments of Diagnostic Radiology, Biomedical Engineering, and Neurosurgery, Yale University, Connecticut, U.S.A.*

Abstract - Magnetic Resonance Driven Electrical Impedance Tomography (MRDEIT) is an Electrical Impedance Tomography (EIT) method that uses magnetic resonance (MR) phenomena for generating the current source and uses the receive sensitivity field as the basis for computing the conductivity and permittivity maps. This paper reports a phantom study that uses a four electrode phantom filled with saline solution. The result shows that MRDEIT can be used to reconstruct conductivity images from electric field measurements.

1. Introduction

Magnetic Resonance Driven Electrical Impedance Tomography (MRDEIT, Negishi *et al.* 2011) is an Electrical Impedance Tomography (EIT) method (Metherall *et al*. 1996, Cheney *et al*. 1999) that uses magnetic resonance (MR) phenomena for generating the current source and performs either electric field measurements or magnetic field measurements for the image acquisition. Unlike MREIT (Zhang 1992, Woo *et al*. 1994, Birgul and Ider 1995), which uses MR in the detection mechanism, MRDEIT uses MR for current induction. MRDEIT is similar in spirit to Electrical Property Tomography (Haacke *et al*. 1991, Katscher *et al*. 2009) in that it utilizes MR as the sole source of imaging. However, MRDEIT differs from EPT in that it may utilize electrical field measurement and that it is based on the sensor field measurement rather than the transmit field measurement. The theory of MRDEIT and computer simulations were described in Negishi *et al*. (2011). The current paper presents a phantom experiment of MRDEIT that is based on the electric field measurement.

2. Method

(1) Measurement

A 12^3[cm^3] cubic EIT phantom that has acrylic walls filled with saline solution, with four copper screw electrodes at 8 [cm] from the bottom was constructed for this experiment (Fig. 1). Within the phantom was a glass bottle (4cm inner diameter, 5mm thick) that was filled with saline solution (possibly with a different concentration). The phantom was connected to a in-house made coil interface which shunted the electrode input during the body coil B1 transmit. The coil interface in turn was connected to the receiver coil socket on a 3T MRI system (Siemens Trio, Erlangen, Germany).

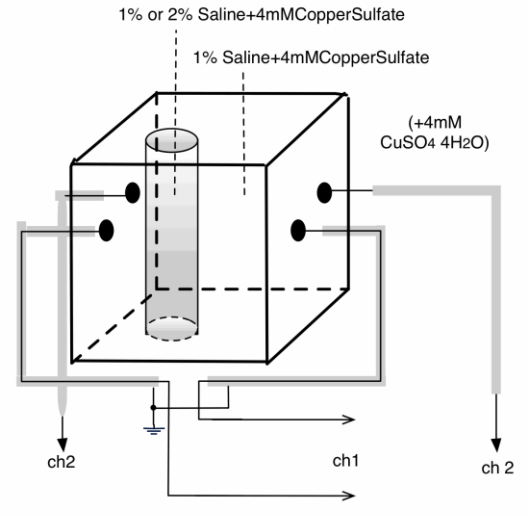

Figure 1. A four electrode, two channel MRDEIT phantom used for the experiment.

A T1 flash sequence (TR/TE=3000/5 ms, FA=90, 25 5mm-slices, 128x128 matrix) was used for the MRDEIT acquisition. The same sequence was used for acquiring a regular body coil image for preprocessing. For both the electrode measurement and the body coil measurement, imaging was performed in two conditions: (1) baseline condition: the whole phantom including the inner bottle was filled with 1% saline and 4 mMol copper sulfate. (2) altered condition: salt was added to the inner bottle to change the saline concentration to 2%. The solution was thoroughly mixed and the phantom stayed in the scanner for 15 minutes before the imaging.

(2) Preprocessing

Regular MR reconstructions were carried out using the signals from the electrodes as the input, resulting in two complex valued 3D images corresponding to the two pairs of electrodes for each condition. Note that these images are not conductivity images but are inputs to the conductivity image reconstruction process described below. Each (complex) voxel intensity value in these images is the signal measured through the electrode corresponding to the particular, frequency and phase encoded excitation of the voxel.

These images were divided voxel-wise by the body coil intensity image to cancel the transmit coil sensitivity and possible T1 and T2 contrast. Proton density contrast in this particular setting was estimated to be 0.26% and was thus neglected. A voxel in the corrected image reflects the electrode sensitivity field, which in turn reflects the electromagnetic property of the saline solution between the excited voxel and the electrodes.

(3) Conductivity reconstruction

The conductivity image was reconstructed from the body coil-corrected image using one iteration of the optimization process described in Negishi *et al*. (2011), which is briefly mentioned here.

The electric field corresponding to a voxel excitation *(i)* is described by a harmonic wave equation

$$\nabla \times \nabla \times \vec{e}^{(i)}(r) - k^2(r)\vec{e}^{(i)}(r) = -\nabla \times \vec{m}^{(i)}(r) \quad (1)$$

$$wave\ number\ k = \sqrt{m\hat{e}(r)w}$$

where $\vec{m}^{(i)}(r)$ is the rotating magnetic field at the position r due to the *(i)*-th voxel excitation, $\vec{e}^{(i)}(r)$ is the electric field vector due to the same excitation, k is the wave number that depends on the electromagnetic properties of the matter and the frequency (μ: the permeability which is assumed to be constant, ε: the complex permittivity, ω: the angular Larmor frequency). This equation is discretized using the Finite Element Model (FEM) that minimizes the energy function with respect to the electric field (Volakis *et al*. 1998).

$$\left(S - TQ\right)e^{(i)} + Ue^{(i)} + Vm^{(i)} = 0 \quad (2)$$

In this equation, S is the matrix representing the double curl term in the wave equation, TQ is a matrix that reflects the term with the wave number where Q is a diagonal matrix whose diagonals are squared wave number of the FEM bases, U is a term corresponding to the second order absorbing boundary condition, and V is a matrix that reflects the driving term on the right hand side of the wave equation. The output from the electrodes are computed from a linear combination of the electric fields.

$$o^{(i)} = Le^{(i)}$$

$$= -L\left(\left(S - TQ\right) + U\right)^{-1} Vm^{(i)} \quad (3)$$

In this equation, L is a matrix that defines the output signal by taking linear combinations of the electric field. Since Q has a diagonal element for all the FEM bases, and also because the complex permittivities are assumed to be isotropic in the current model, Q is highly redundant. To simplify the complex permittivity reconstruction, a vector q whose length is the number of elements in the FEM model is defined. Also, the concatenation of output signal values from all the excitations $o = \left[o^{(1)}\ o^{(2)} \ldots o^{(N)} \right]$ (N is the number of considered voxel excitations) is defined. Finally, the vector q is obtained by iterative applications of linear least squared error estimates to minimize the difference between the measured output signals and the estimated output signals:

$$\Delta q = \left(\left(\partial o / \partial q \right)^H \left(\partial o / \partial q \right) + \lambda I \right)^{-1} \left(\partial o / \partial q \right)^H \Delta o \quad (3)$$

where λ is a regularization constant (0.01 in the current paper). See Negishi *et al*. (2011) for the explicit formula for computing the Jacobian matrix. Equation (3) is applied repeatedly, re-computing the Jacobian matrix each time to obtain progressively better estimates of the complex permittivity until the update process converges. However, this equation was applied only once in the current study.

Before applying equation (3) to the experimental data, the (two-channel) images in the baseline condition were scaled to have the same average magnitudes as those of the simulated output voltages, and the same scaling factors were applied to the altered condition images.

3. Results

Figure 2 shows the reconstructed conductivity images of the slices near the electrodes. Only six slices centered around the electrodes (5 mm interval) are shown, since conductivity changes on other slices were not detected.

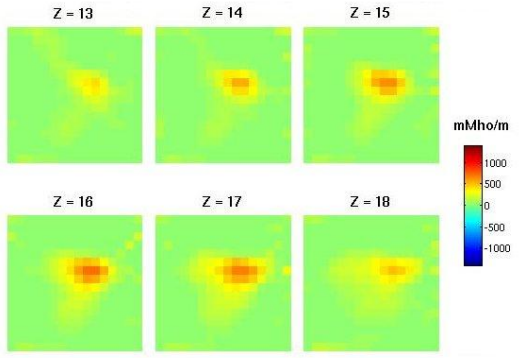

Figure 2. Reconstructed conductivity difference image. Top view of the reconstructed conductivity image of the saline in Figure 1.

4. Discussion and conclusion

It can be seen that high conductivity region is correctly detected near the electrodes (Z=14 to 18). However, the shape of the region is not satisfactorily reconstructed. Furthermore, conductivity changes far away from the electrodes are not well detected. The cause of these problems may be (1) a small number of electrodes, (2) a low spatial resolution FEM modeling, and (3) a low signal to noise ratio of signals from the electrodes.

It could be argued that the leads from the electrodes and possibly the saline solution form coils, and thus the recorded signals arise from conventional magnetic induction rather than from the electric field component. However, it was experimentally observed that while the leads do form loops through the conducting media, they do not pick up the MR signals because they are perpendicular to the B0 direction. This could be confirmed by comparing the reconstructed MR images from the electrodes in the above setting and the same image from a 90 degrees rotated (in the transverse plane) phantom (Figure 3). The former showed a pattern

characteristic of the electric field predicted from the wave equation, most notably with dark planes that are perpendicular to the B0 field and include the measurement electrodes. The latter showed a profile typical of surface coils, without dark planes and showing the bright area only below the electrodes, since only that part of the phantom is within the loop.

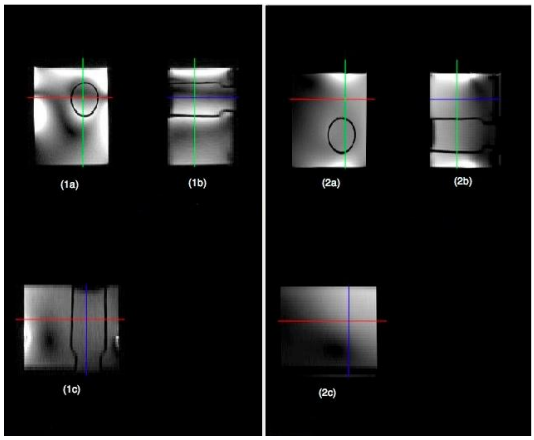

Figure 3. The MR intensity images recorded from one pair of electrodes in the phantom with the original orientation (left) and with 90 degrees-rotation in the horizontal plane (right). Note the dark lines along the red cursor in (1a) and the blue cursor in (1b), and the darkness in the right half (corresponding to the upper part of the inner bottle) in (2b).

In summary, the phantom experiment validated the theory of MRDEIT. Technical problems were identified for achieving a higher spatial resolution.

References

Birgul O, Ider YZ (1995) Use of the magnetic field generated by the internal distribution of injected currents for electrical impedance tomography, in *Proc. IXth Int. Conf. Elec. Bio-Impedance, Heidelberg, Germany*, 418–419.

Cheney M, Isaacson D, Newell JC (1999) Electrical impedance tomography, *SIAM Rev.,* **41**, 85–101.

Haacke EM, Petropoulos LS, Nilges EW, Wu DH, (1991) Extraction of conductivity and permittivity using magnetic resonance imaging, *Phys. Med. Biol*., **36**, 723–733.

Katscher U, Voigt T, Findeklee C, Vernickel P, Nehrke K, Dössel O (2009) Determination of electric conductivity and local SAR via B1mapping, *IEEE Trans. Biomed. Eng.* **28** (9) 1365–1374.

Metherall P, Barber DC, Smallwood RH, Brown BH (1996) Three dimensional electrical impedance tomography, *Nature*, **380**, 509–512, 1996.

Negishi M, Tong T, Constable RT (2011) Magnetic resonance driven electrical impedance tomography: a simulation study. *IEEE Trans Med Imaging* **30** (3): 828-37.

Volakis JL, Chatterjee A, Kempel LC (1998) *Finite Element Methods for Electromagnetics*, IEEE Press, NY.

Woo EJ, Lee SY, Mun CW (1994) Impedance tomography using internal current density distribution measured by nuclear magnetic resonance, in *Proc. SPIE*, 1994, **2299**, 77–385.

Zhang N (1992) Electrical impedance tomography based on current density imaging, *M.S. thesis, Dept. Elec. Eng., Univ. Toronto, Toronto, Canada*.